A Lateral-Axis Microelectromechanical Tuning-Fork Gyroscope With Decoupled Comb Drive Operating at Atmospheric Pressure

Zhong Yang Guo, Long Tao Lin, Qian Cheng Zhao, Zhen Chuan Yang, Huikai Xie, *Senior Member, IEEE*, and Gui Zhen Yan

***Abstract*—In this paper, a silicon bulk micromachined lateral-axis tuning-fork gyroscope (TFG) with a decoupled comb drive and torsional sensing comb capacitors is presented. The novel driving comb capacitors are used to suppress the parasitic out-of-plane electrostatic force and, hence, can decouple the mechanical crosstalk from the sensing mode to the driving mode in a simple manner. The torsional sensing combs are designed to differentially sense the out-of-plane rotational moment and are arranged centroidally to be immune to fabrication imperfections for good linearity and electrostatic force balancing. The torsional sensing combs adopted in the TFG help to lower the air damping of the sensing mode while the driving mode of the gyroscope is dominated by slide-film air damping; hence, it can work even at atmospheric pressure. The process for this lateral-axis gyroscope can also be used to fabricate z-axis gyroscopes; therefore, low-cost miniature monolithic inertial measurement units can be realized without vacuum packaging. The TFG is tested at atmospheric pressure with a sensitivity of 17.8 mV/°/s and a nonlinearity of 0.6% in a full-scale range of 1000°/s. The bias stability is measured to be $0.05°/\mathrm{s}\ (1\sigma)$ in 30 min with an equivalent noise angular rate of 0.02°/s/Hz$^{1/2}$. [2009-0229]**

***Index Terms*—Decoupling, gyroscopes, lateral-axis gyroscopes, microelectromechanical systems (MEMS), out-of-plane motion sensing, tuning-fork gyroscopes (TFGs).**

I. Introduction

ALTHOUGH there are still great gaps between the performances of micromachined and traditional gyroscopes such as the ring-laser, fiber-optic, and dynamically tuned rate gyroscopes, micromachined gyroscopes have attracted more and more attention in recent years [1]. Gyroscope application fields are greatly extended because of micromachined gyroscopes' low cost, small size, and low power consumption [2]. Micromachined gyroscopes experienced rapid progress in the past two decades particularly with the utilization of the comb drive [3]–[5]. Several microelectromechanical system (MEMS) gyroscopes have been commercialized [6]–[9]. As for structure designs, tuning-fork gyroscopes (TFGs) are the most popular choices since TFGs can realize differential Coriolis acceleration sensing to improve the sensitivity and linearity as well as to suppress the sensitivity to linear accelerations [4], [5], [9], [10]. However, most of the previously reported lateral-axis TFGs use parallel-plate capacitors to sense the out-of-plane motion, which needs high-cost vacuum packaging to obtain good performance.

As one of the main error sources of a micromachined gyroscope, the mechanical coupling or crosstalk between the driving and sensing modes must be suppressed [11]–[19]. Three kinds of methods have been developed to reduce such mechanical couplings. The first, called mechanical insulation here for convenience, is a pure mechanical method that employs independent beams and extra masses or frames to isolate the two modes mechanically. This method was first proposed by Geiger *et al.* [11], and several different gyroscopes using such method were reported [11]–[13]. Mechanical insulation can efficiently decouple the drive-to-sense (DTS) mechanical coupling and has been widely adopted in many MEMS gyroscopes [9], [11]–[13], [17], [19]. The second method is named electrostatic-force compensation which adopts electrostatic forces to adjust the misalignment of the driving mode [5], [14]–[17]. Kawai *et al.* employed an adjustable dc bias voltage to reduce mechanical coupling [14], Sharma *et al.* used force-feedback balancing circuits to null the quadrature error in their z-axis TFG [5], and Park and Horowitz and Painter and Shkel proposed adaptive control and self-calibration methods, respectively, to suppress the coupling [15]–[17]. However, the methods using dc bias voltage and feedback control are sensitive to parameter variations [15], while the adaptive control and self-calibration schemes increase the complexity of the control system. The third method is mechanical trimming which utilizes laser or focused ion beams to trim the spring beams or proof mass so as to change the stiffness and/or adjust the vibration imbalance [9], [18]. The disadvantage of such post-trimming method is that it is time consuming and unsuitable for batch production [16].

Moreover, the DTS mechanical coupling that causes quadrature error has been paid much attention, but the sense-to-drive (STD) mechanical coupling, another nonideal sensor behavior [13], has not been well investigated particularly for TFGs [4],

Manuscript received September 21, 2009; revised January 13, 2010; accepted February 24, 2010. Date of publication April 26, 2010; date of current version June 3, 2010. This work was supported in part by the National Natural Science Foundation of China under Grant 50575001, in part by the National High Technology Research and Development Program of China under Grant 2006AA04Z371, and in part by the Chinese Government Scholarships for Postgraduates. Subject Editor M. Wong.

Z. Y. Guo, L. T. Lin, Q. C. Zhao, Z. C. Yang, and G. Z. Yan are with the Institute of Microelectronics, Peking University, Beijing 100871, China (e-mail: zhongyguo@gmail.com).

H. Xie is with the Department of Electrical and Computer Engineering, University of Florida, Gainesville, FL 32601 USA.

Color versions of one or more of the figures in this paper are available online at http://ieeexplore.ieee.org.

Digital Object Identifier 10.1109/JMEMS.2010.2046477

[5], [10]. Geiger *et al.* used the mechanical insulation method to decouple both the DTS and STD couplings, resulting in a doubly decoupled gyroscope with one proof mass [13], [19]. However, decoupling both the DTS and STD couplings using mechanical insulation requires a sophisticated structure [19]. Furthermore, since the out-of-plane motion is involved, such doubly decoupled structures become even more complicated for lateral-axis gyroscopes which are key components in triaxial monolithic gyroscope integration and miniature inertial measurement units (IMUs) [2], [20].

In order to realize lateral-axis TFGs that can operate at atmospheric pressure, low-damping out-of-plane displacement-sensing capacitors are needed. The commonly used gap-variable capacitors not only have drawbacks of small dynamic range and possible pull-in instability when open-loop sensing is used but also have large squeezed-film air damping [21]. Therefore, they are not suitable for sensing at atmospheric pressure. On the other hand, for overlap-area-changing mechanisms, large gaps between the proof mass and the substrate can be used to lower the squeezed-film damping without sacrificing the sensitivity; thus, a large dynamic range can be achieved. Several kinds of comb capacitors have been developed for out-of-plane displacement sensing using overlap-area-changing mechanisms, some of which were designed to sense the displacements differentially by carefully arranging the comb fingers [20]–[24], [27]–[33]. Selvakumar and Najafi reported a comb capacitor to sense the torsional out-of-plane motion of a z-axis accelerometer, but it can neither distinguish the acceleration directions nor sense the rotational displacement differentially [21]. A rotational sensing comb capacitor with different thicknesses of neighboring fingers at the lower side has been developed in our previous work to sense the out-of-plane displacement differentially [20], [22]. A similar vertical comb capacitor was also proposed by Tsuchiya and Funabashi [23], where the thicknesses of neighboring fingers are different at the upper side. Although such capacitors can differentially sense vertical motion, they have large nonlinearity [23]. Xie and Fedder also reported a vertical comb capacitor formed by multi-thin-film structures fabricated by a CMOS-MEMS process [24], but it has the disadvantages of small capacitance and large temperature sensitivity.

Novel vertical or torsional comb capacitors with rotor and stator fingers having the same thickness but different vertical positions have been used either as vertical actuators to obtain large out-of-plane displacement [25], [26] or as vertical or torsional sensors to further improve the linearity of out-of-plane sensing comb capacitors [27]–[33]. However, the gyroscope reported in [29] and [30] is structurally asymmetrical and, hence, in principle, is sensitive to z-axis acceleration. The gyroscope in [27] and [28] has the same issue. In our more recent designs [31]–[33], symmetrical lateral-axis MEMS gyroscopes with torsional sensing combs were proposed, but the proof mass of the gyroscope in [31] and [32] is relatively small and the beams are double clamped. The thinning of the movable drive combs in [33] results in a large critical dimension (CD) loss and poor reliability.

In this paper, by adopting the torsional sensing comb capacitor design reported in [31]–[33] and introducing a special driving comb capacitor design, a lateral-axis TFG that can decouple both DTS and STD mechanical couplings and operate at atmospheric pressure is presented. Moreover, folded sensing beams are used to provide the freedom of out-of-plane torsional displacements for the gyroscope. Because of its symmetric structure and the arrangement of the torsional sensing comb capacitors, the TFG can detect the out-of-plane rotation differentially and be insensitive to external acceleration disturbances. Furthermore, the centroidal topology of the torsional sensing combs makes the TFG have good linearity with large full-scale range even if some fabrication imperfections exist. The silicon-on-glass (SOG) process for the TFG is also fully compatible with the z-axis gyroscope process [27]–[34].

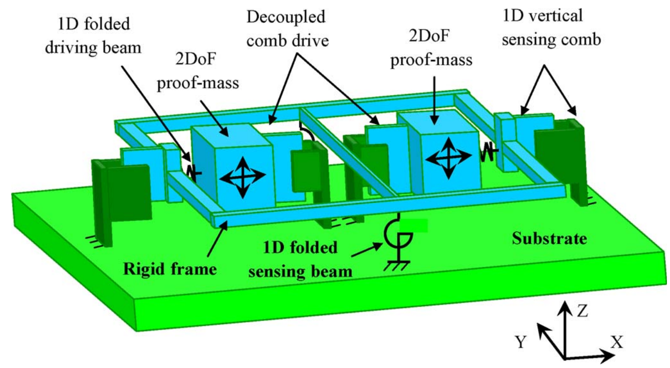

Fig. 1. Schematic diagram of the TFG.

This paper is organized as follows. The design and working principle of the TFG will be described in Section II, where the decoupling principle and decoupled comb drive as well as the torsional sensing capacitors used in the TFG will be discussed in detail. Section III briefly introduces the fabrication process, and test results will be given in Section IV followed by the conclusion in the last section.

II. Topology Design and Working Principle

A. Structure and Operational Principle of the TFG

The schematic of the presented TFG is shown in Fig. 1. It is a symmetrical structure with dual proof masses. The movable comb fingers of the comb drives are rigidly connected with the proof masses which are connected to a gimbal through several driving beams. The movable sensing comb fingers are rigidly connected to the gimbal which is linked to the anchors via four sensing beams. The two proof masses are electrostatically actuated to vibrate in opposite directions along the x-axis. When there is an external rotation about the y-axis, the induced Coriolis acceleration will force the proof masses to vibrate oppositely along the z-axis and the torsional comb capacitors can differentially sense the displacement.

The folded sensing beams are adopted to provide the freedom of out-of-plane rotational displacements for the gyroscope. The folded sensing beams are important for the TFG to obtain high linearity, large dynamic range, and good bias stability because they can release residual stresses [3], [4], [35].

Although high working frequencies are helpful to reduce vibration and acoustic effects, high resonant frequencies also reduce the sensitivity or require higher driving voltage particularly for those operating at atmospheric pressure [2], [16]. In

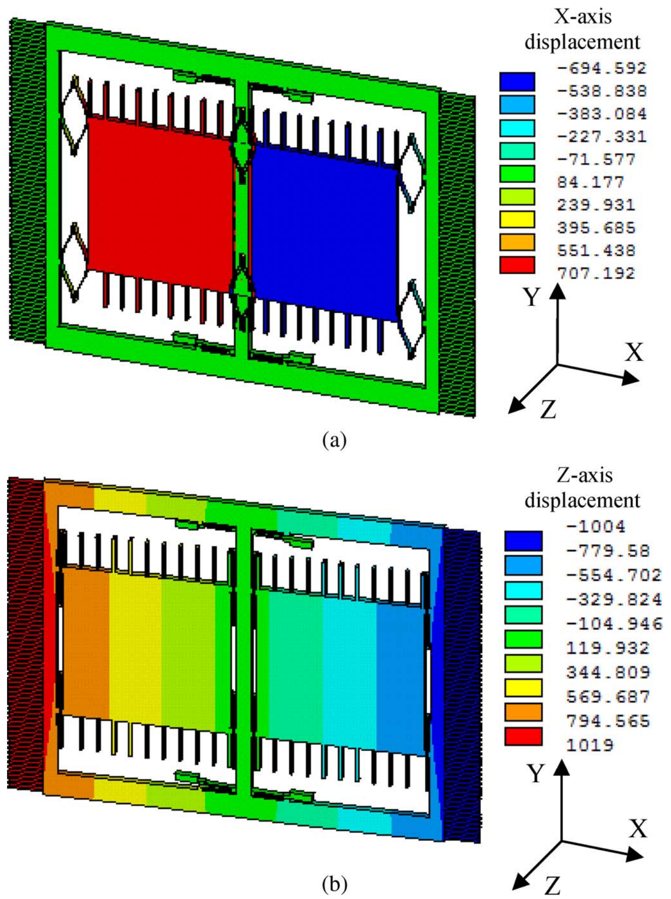

Fig. 2. Working-mode simulation by ANSYS. (a) Driving mode (frequency = 3.23 kHz). (b) Sensing mode (frequency = 3.33 kHz).

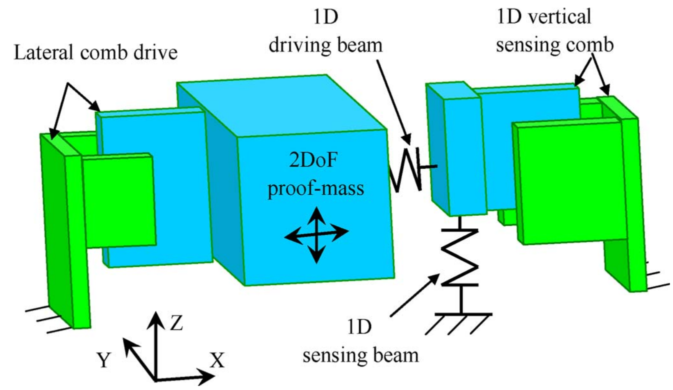

Fig. 3. Schematic diagram of the decoupling principle used in the TFG.

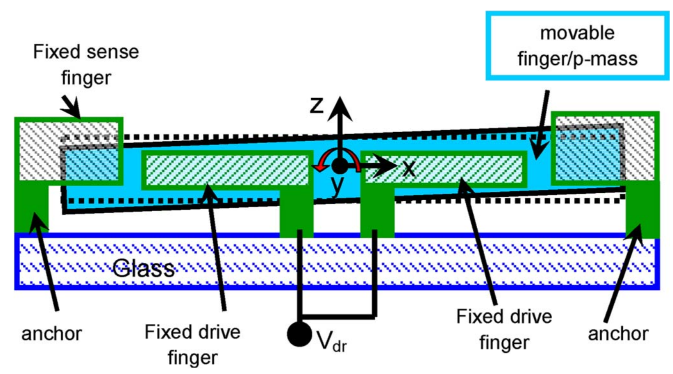

Fig. 4. Schematic sectional view of the TFG.

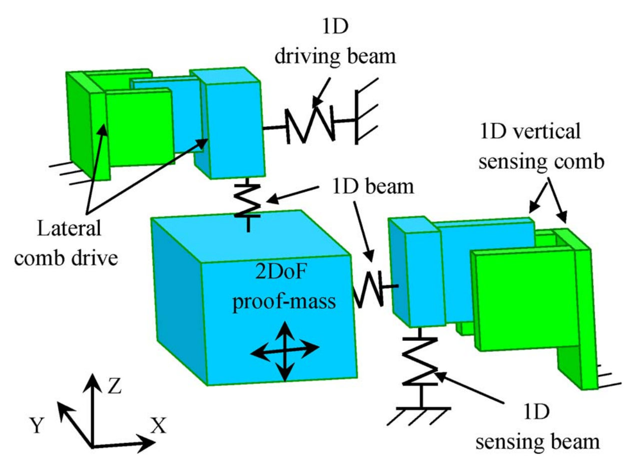

Fig. 5. Schematic diagram of the doubly decoupling principle [13] adopted in a lateral-axis gyroscope.

order to achieve high sensitivity, the working frequencies are designed to be about 3 kHz which are just above the typical environmental noise bandwidth (> 2 kHz) [2]. The driving and sensing modes are simulated using ANSYS, as shown in Fig. 2. The driving and sensing mode frequencies are 3.23 and 3.33 kHz, respectively.

B. Decoupling Principle

Two different decoupling methods are adopted in the proposed TFG. The DTS mechanical coupling is suppressed using the aforementioned mechanical insulation while the STD mechanical coupling is decoupled through the newly designed decoupling comb drive. The decoupling principle of the TFG is schematically shown in Fig. 3. Fig. 4 shows the schematic sectional view of the TFG to illustrate the decoupling principle of the proposed comb drive in the device.

As shown in Figs. 3 and 4, the movable driving fingers together with the proof mass are electrostatically driven to resonate in the x-axis but the movable sensing comb will not vibrate because of the constraint of the 1-D sensing beam. Therefore, the sensing mode is decoupled from the driving mode when there is no angular rate input. Upon a y-axis angular rate input, the proof mass will vibrate along the z-axis because of the induced Coriolis force and, at the same time, force the movable sensing comb to move together. The movable driving comb will also move with the proof mass along the z-axis in the sensing mode since they are rigidly connected. As the movable fingers are symmetrically higher than the fixed comb fingers, when the displacement along the z-axis is within a certain range, there will be almost no changes in the capacitance of the comb drive. Therefore, nearly no electrostatic force along the z-axis is applied on the movable driving comb. Hence, the STD mechanical coupling can be suppressed. A detailed analysis and discussion of this decoupling method will be given in the following section.

As a comparison, the doubly decoupling principle based on mechanical insulation in a lateral-axis gyroscope is schematically shown in Fig. 5, which is adopted from [19] and [27]–[31].

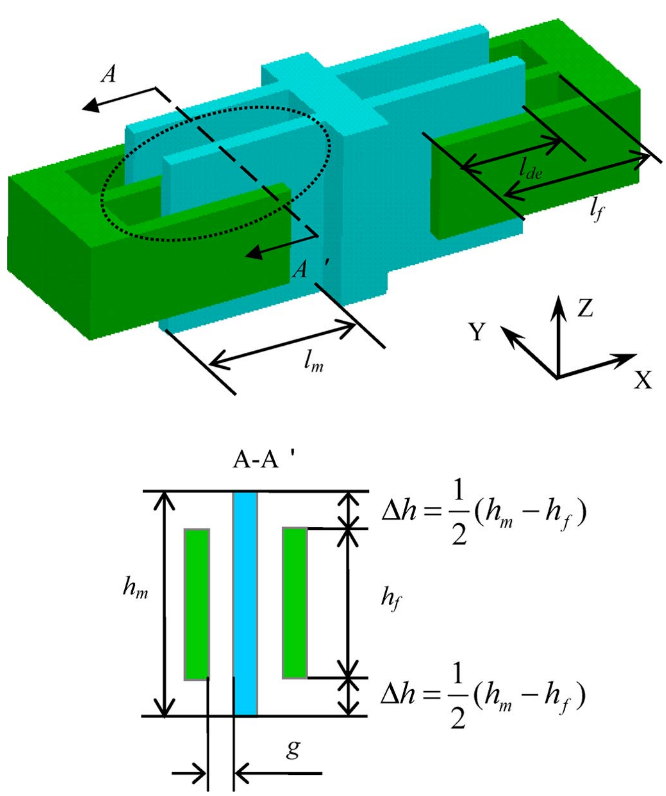

Fig. 6. Schematic of the comb drive and the sectional view of one unit.

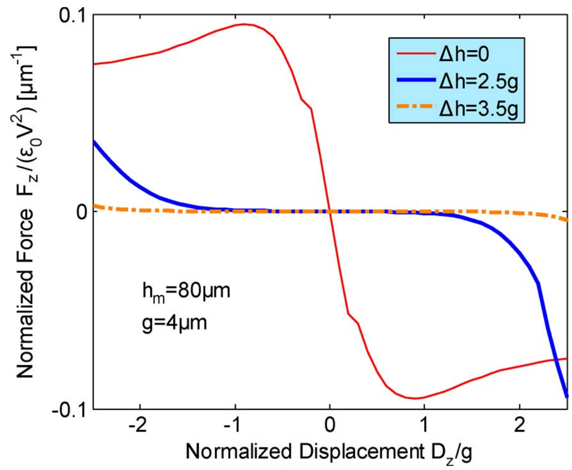

Fig. 7. Normalized z-axis force versus the normalized out-of-plane displacement.

The movable comb of the comb drive together with the proof mass is electrostatically actuated to resonate in the x-axis. Because of the constraint of the sensing beam, the movable sensing comb will not vibrate in the x-axis; thus, the DTS mechanical coupling can be suppressed. Under an angular rate along the y-axis, the proof mass will vibrate along the z-axis because of the induced Coriolis force and will force the movable sensing comb to move together through the 1-D beam between the proof mass and the movable sensing comb. However, the movable comb of the comb drive cannot vibrate along the z-axis due to the constraint of the 1-D driving beam. Hence, the STD mechanical coupling can be decoupled.

From Figs. 3 and 5, a conclusion can be drawn: Reducing the STD coupling by the decoupled comb drive has two advantages over the mechanical insulation method mentioned previously. First, it can simplify the structure of the device particularly for lateral-axis gyroscopes because two groups of 1-D beams and the driving mass [13] become unnecessary in the decoupled comb drive design. Second, the movable driving combs are also parts of the proof masses; therefore, the total mass is increased, which helps to improve the sensor performance particularly for those working at atmospheric pressure where many groups of comb drives are needed to obtain large vibration amplitude. For the lateral-axis TFG proposed in this paper, the mass of the comb drive is about 10% that of the proof mass.

C. Decoupled Comb Drive Design

The schematic of the proposed comb drive is shown in Fig. 6. The height of the movable driving comb fingers h_m is symmetrically higher/lower than the height of the fixed comb fingers h_f by Δh on both top and bottom sides. By properly choosing Δh, there will be no disturbing electrostatic force between the fixed and the movable driving comb fingers along the z-axis induced by the drive voltage V. Thus, in the first-order approximation, the STD coupling can be completely eliminated.

Fig. 7 shows the normalized z-axis force versus the normalized out-of-plane displacement under different values of Δh. While the normalized driving force $F_{\mathrm{dr}}/(\varepsilon_0 V^2) = 0.25\ \mu\mathrm{m}^{-1}$ for $g = 4\ \mu$m, the forces are calculated based on the equations in [36].

As shown in Fig. 7, the normalized force $F_z/(\varepsilon_0 V^2)$ for the combs with equal height ($\Delta h = 0$) is inconstant and substantially large when compared with the desired driving force, which will deteriorate the performance of a gyroscope if it is not suppressed efficiently.

With the increase of Δh, $F_z/(\varepsilon_0 V^2)$ decreases and becomes zero when the normalized displacement D_z/g is within a certain range. Furthermore, the zero-force range increases with increasing Δh. Thus, the disturbing electrostatic force F_z can be efficiently suppressed by carefully choosing the parameters of the comb drive. For example, F_z can be neglected when $\Delta h \geq 2.5g$ and $D_z/g \in (-0.5, 0.5)$. One can also come to the same conclusion by simulation using numerical tools such as ANSYS [37].

Higher aspect ratio structures can increase the proof mass and thus improve the resolution and stability of the device, but they also increase the difficulty of fabrication. Based on the SOG process developed at Peking University (PKU), fine silicon structures can be fabricated when the minimum gap is 4 μm and the aspect ratio is within 20. Therefore, the gap of the neighboring fingers of the comb drive is selected to be 4 μm, and the thickness of the movable comb fingers and the width of all the drive fingers are taken as $h_m = 80\ \mu$m and $w_{\mathrm{dr}} = 80\ \mu$m, respectively. Hence, $\Delta h = 10\ \mu$m can be selected in the TFG.

The length of the finger $l_m = l_f$ and the initial engaged length of the fingers l_{de} are designed not only to allow a large travel range for the proof masses but also to keep a constant force–voltage relationship even when acceleration is present. In the proposed TFG, a travel range of $\pm 10\ \mu$m is designed

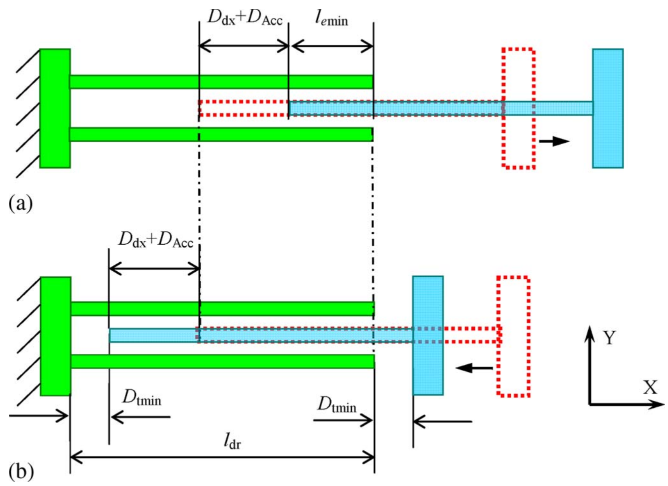

Fig. 8. Length design of the drive comb.

TABLE I
MAIN PARAMETERS OF THE COMB DRIVE (IN MICROMETERS)

w_{dr}	g	h_m	h_f	l_{de}	$l_m(l_f)$
5	4	80	60	20	50

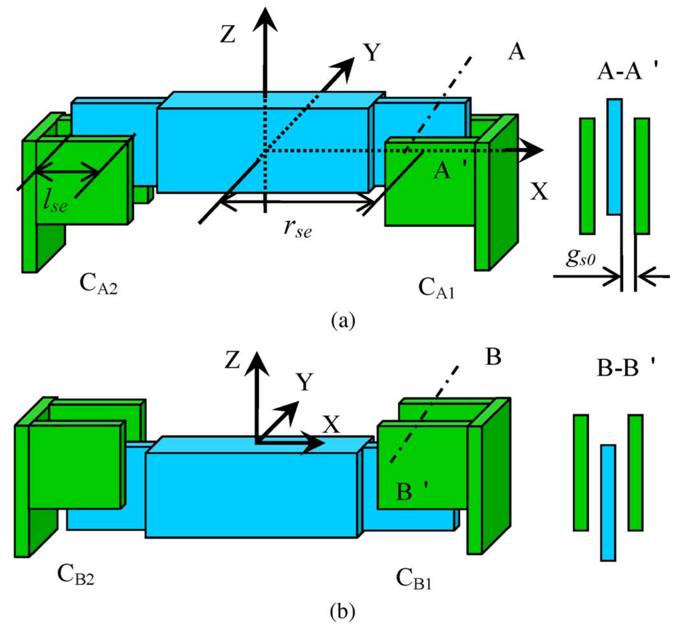

Fig. 9. Two types of torsional sensing combs: (a) type A and (b) type B.

for the proof masses. As shown in Fig. 8(a), the minimum engaged length $l_{e\,\min}$ can be set to $2g$ in order to obtain a constant force–voltage relationship when the movable finger has the maximum x-axis displacement [33]. On the other hand, the electrostatic force at the tips of the fingers should be small enough when the movable finger has a maximum $-x$-axis displacement, as shown in Fig. 8(b). Therefore, the minimum distance $D_{t\,\min}$ can be given by

$$D_{t\,\min} > 10\left(\frac{w_{\mathrm{dr}}g}{\delta}\right)^{\frac{1}{2}} \tag{1}$$

where $\delta = F_{\mathrm{ct}}/F_{\mathrm{dr}} \times 100$ and F_{ct} and F_{dr} are the electrostatic force at the finger tips and the drive force, respectively. Considering the operating environment such as external acceleration, the initial engaged length l_{de} can be expressed as

$$l_{\mathrm{de}} > l_{e\,\min} + 2D_{\mathrm{dx}} + 2D_{\mathrm{Acc}} \tag{2}$$

where D_{dx} is the displacement of the movable finger, $D_{\mathrm{Acc}} = Acc/(2\pi\omega_d)^2$ is the displacement caused by acceleration Acc, and $\omega_d = 3.23$ kHz is the resonate frequency of the driving mode of the TFG.

Therefore, the length of the drive finger $l_m = l_f = l_{\mathrm{dr}}$, and

$$l_{\mathrm{dr}} > l_{e\,\min} + 2D_{\mathrm{dx}} + 2D_{\mathrm{Acc}} + D_{t\,\min}. \tag{3}$$

When $\delta = 5$ and $Acc = 50G$ (G is the gravitation acceleration), l_{de} and l_{dr} are 20 and 50 μm, respectively. The main parameters of the comb drive are listed in Table I.

D. Torsional Sensing Comb

The torsional sensing comb design in this TFG can differentially detect the rotational displacement induced by Coriolis acceleration. It is also robust and insensitive to fabrication imperfections. Moreover, the torsional sensing fingers are arranged to balance the electrostatic force induced by the bias voltage on the sensing electrodes.

To differentially detect the out-of-plane rotational displacements, two types of torsional sensing combs can be used, which are shown in Fig. 9. The thickness of the comb fingers are the same but the movable comb fingers are either higher (type A) or lower (type B) than the fixed finger. When the movable comb fingers have a rotational angle of θ, the changes in the capacitances of the two types of combs can be described as [21]

$$\Delta C_A(\theta) = C_{A1}(\theta) - C_{A2}(\theta) = 4\frac{\varepsilon l_{\mathrm{se}}}{g_{s0}}r_{\mathrm{se}}\theta \tag{4a}$$

$$\Delta C_B(\theta) = C_{B1}(\theta) - C_{B2}(\theta) = -4\frac{\varepsilon l_{\mathrm{se}}}{g_{s0}}r_{\mathrm{se}}\theta \tag{4b}$$

where l_{se} is the engaged length of the sense finger, r_{se} is the rotation radius of the center of the engaged finger, and g_{s0} is the gap between neighboring fingers. The fringe capacitances are neglected here.

The changes in the capacitances of the two types of combs can also be simulated using numerical tools such as ANSYS. Fig. 10 shows the simulated result of the increase of type B capacitance versus rotational angle using ANSYS, where $l_{\mathrm{se}} = 425$ μm, $r_{\mathrm{se}} = 237$ μm, $g_{s0} = (4$ μm, and the width, thickness, and height differences in the z-axis of the fingers are 12, 70, and 10 μm, respectively. For comparison, the calculated result using (4b) is also shown in Fig. 10. The difference between the calculated result and the simulated result is small; therefore, it is reasonable to estimate the changes in the capacitances of the combs by (4).

Therefore, both types of combs can differently sense the rotational displacements with respect to the y-axis with good linearity if the rotational angle is within a few degrees.

However, fabrication imperfections normally exist in high-aspect-ratio silicon deep reactive ion etching (DRIE) [38]–[40]. For example, the sidewalls of comb fingers are often not

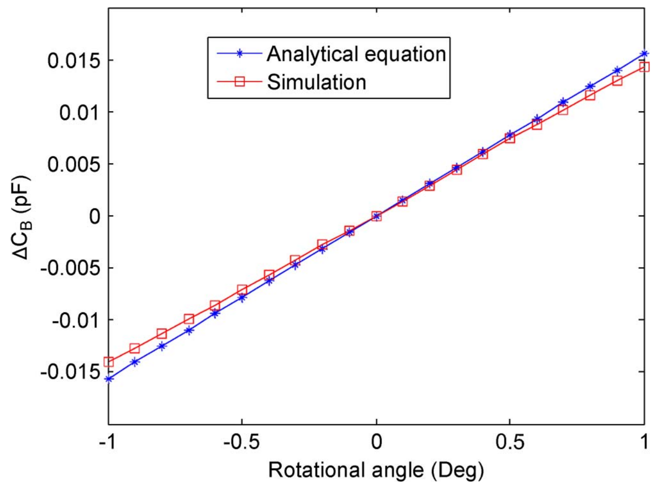

Fig. 10. Increase of the capacitance of the type B comb versus rotational angle.

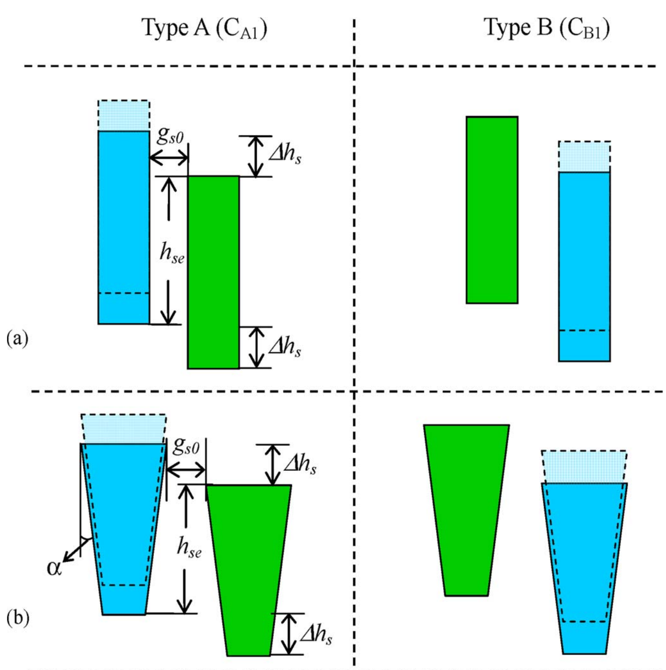

Fig. 11. Sectional views of the comb fingers with different sidewalls. (a) Vertical and (b) upper sides are wider than the bottom side.

perfectly straight. Fig. 11 schematically shows a typical case of torsional comb fingers with sloped sidewalls. By neglecting the fringe capacitance and assuming that the center of the engaged fingers has a ΔZ displacement, the capacitance for the cases in Fig. 11(b) can be expressed as

$$C_{A1}(\Delta z) = \frac{\varepsilon l_{\mathrm{se}}}{\tan\alpha} \ln\left(1 + \frac{2(h_{\mathrm{se}} - \Delta z)\tan\alpha}{g_{s0} + (\Delta h_s + \Delta z)\tan\alpha}\right) \quad \text{(5a)}$$

$$C_{B1}(\Delta z) = \frac{\varepsilon l_{\mathrm{se}}}{\tan\alpha} \ln\left(1 + \frac{2(h_{\mathrm{se}} + \Delta z)\tan\alpha}{g_{s0} + (\Delta h_s - \Delta z)\tan\alpha}\right) \quad \text{(5b)}$$

where g_{s0} and h_{se} are the minimum finger gap and the initial engaged finger height, respectively.

Fig. 12 shows the relative changes of the capacitances $\Delta C/C(0)$ calculated using (6) when $\alpha = 2^\circ$. If the two types of combs are combined, such as $C_{c1} = -C_{A1} + C_{B2}$, the linearity of the capacitance changes of C_{c1} will be more immune to the fabrication imperfections than that of the capacitors composed of only one type of torsional comb. As shown in Fig. 12, the nonlinearity is reduced from 0.4% down to 0.04%.

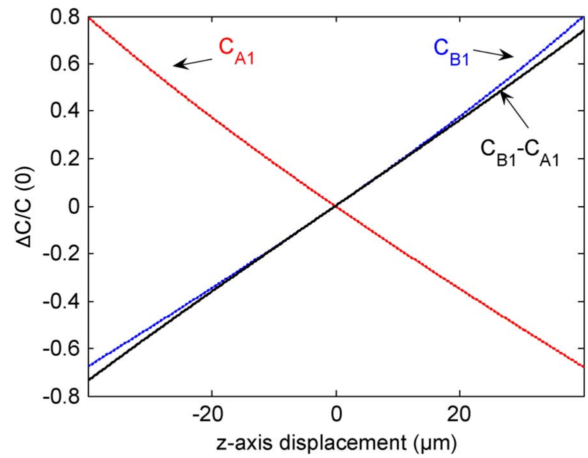

Fig. 12. Relative changes of the capacitances.

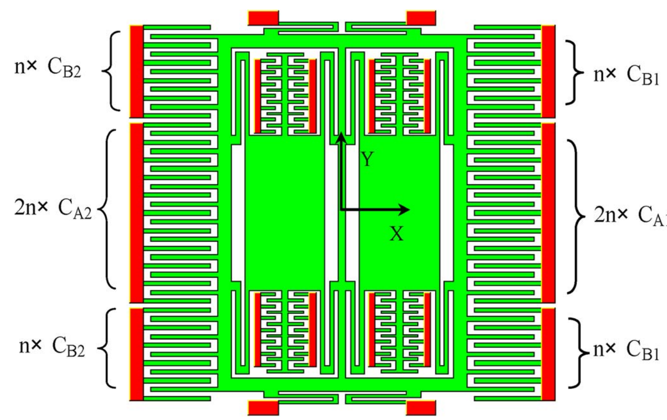

Fig. 13. Topology of the sensing comb.

Furthermore, in order to make the capacitors insensitive to rotational displacements with respect to the x-axis, the two types of combs are arranged symmetrically with a centroidal topology, as shown in Fig. 13.

For such an arrangement, the changes in total sensing capacitance C_s caused by a rotation about the y-axis can be written as

$$\Delta C_s = 2n\left[(C_{A1} + C_{B2}) - (C_{A2} + C_{B1})\right] \quad (6)$$

or

$$\Delta C_s = 2n\left[(C_{A1} - C_{A2}) + (C_{B2} - C_{B1})\right]. \quad (7)$$

Equation (6) indicates that the torsional combs with such an arrangement can differentially detect the rotational displacement with respect to the y-axis while (7) shows that C_s does not change with the displacements of the movable fingers along the x-axis.

Moreover, the electrostatic force along the z-axis induced by the bias voltage on the sensing electrodes is also balanced by such an arrangement. The cross-sectional view of the sensing

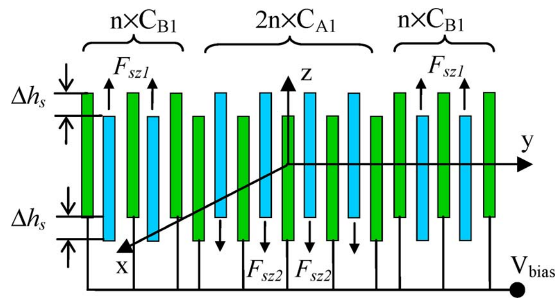

Fig. 14. Schematic sectional view of the sensing fingers.

TABLE II
MAIN PARAMETERS OF THE SENSING COMB (IN MICROMETERS)

w_{dr}	g_{s0}	t_s	Δh_s	l_s	l_{se}
12	4	70	10	450	425

fingers is schematically shown in Fig. 14. All the fingers have the same thicknesses but different heights with a height difference of Δh_s. In order to balance the electrostatic force in the z-axis, the overall layout of all the fingers is symmetric with respect to the y-axis, as shown in Fig. 14. When a voltage is applied to the sensing comb, electrostatic forces will be generated along the z-axis, i.e., F_{sz1} and F_{sz2}, as shown in Fig. 14. These two forces will be equal and counteracted. Thus, the net electrostatic force, $F_{sz} = F_{sz2} + F_{sz1}$, is zero. According to [33] and for the sake of the compatibility of the fabrication processes with that of the decoupled comb drive, Δh_s is also 2.5 times the finger gap, i.e., $g_{s0} = 4$ μm. Hence, $\Delta h_s = 10$ μm, and the thickness of the fingers t_s is 70 μm. Based on our previous work and the optimization of the capacitive sensitivity of the TFG, the width w_s, length l_s, and engaged length l_{se} of the sensing fingers are 12, 450, and 425 μm, respectively. The major parameters of the sensing combs are listed in Table II.

E. Other Parameter Designs

The beams and the proof masses have the same thickness of 80 μm, as discussed previously. A proof mass with a large area helps to improve the performance, such as the noise floor of the device, but this may decrease the capacitive sensitivity because a larger proof mass increases the inertia moment of the rotational sensing TFG. The area of the proof mass is 2.1 mm $\times$ 2.4 mm in this design, and the device size is 6 mm $\times$ 7 mm.

In order to decrease the squeeze-film damping, large gaps between the proof masses and the substrate are needed. However, large gaps also increase the difficulty of fabrication of the structures particularly for the decoupled comb drive and the sensing combs. A gap of 30 μm is used in the TFG and other lateral-axis torsional sensing gyroscopes from our group [29]–[33].

The dimensions of in-plane driving and out-of-plane sensing beams are designed according to the proof masses and are listed in Table III.

TABLE III
MAIN PARAMETERS OF THE BEAMS

	Width (μm)	Length (μm)	Thickness (μm)	Total number
Driving beams	10	500	80	16
Sensing beams	25	360	80	4

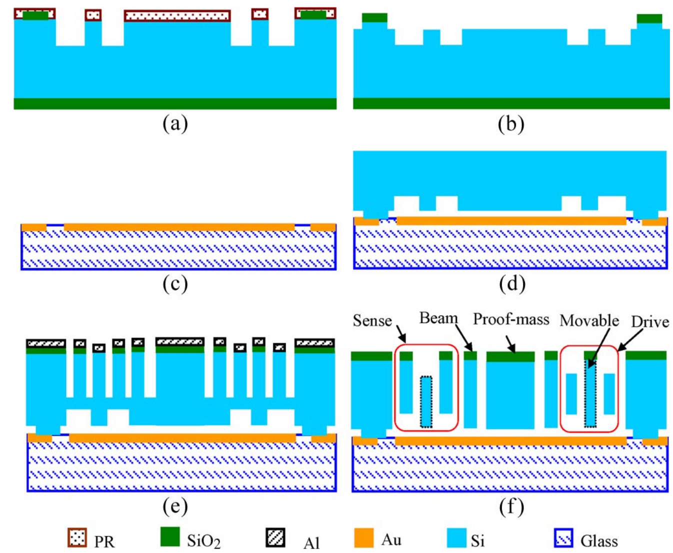

Fig. 15. Main steps of the fabrication process.

III. DEVICE FABRICATION

The TFG with decoupled comb drives and torsional sensing combs can be fabricated using a five-mask SOG process involving silicon/glass wafer bonding and DRIE, which is developed at PKU and has been used in our previous work [1], [27]–[33]. Fig. 15 shows the main steps of the fabrication process. First, the bottom sides of the comb fingers are defined by mask2 and DRIE (a). Then, the spacer between the glass substrate (Pyrex7740) and the proof masses are formed by mask1 and the second DRIE (b). The electrical connections are formed on the glass substrate by a lift-off process using mask3 (c). After anodic bonding and KOH thinning (d), the structure is prereleased by the third DRIE and mask4 (e). Then, the structure is released by the last DRIE and mask5, and the top sides of the fingers are formed at the same time (f).

Although this process needs two more masks than the z-axis gyroscope process reported in [34] to realize the height difference of the comb fingers, the two processes are fully compatible, which makes it applicable for the realization of monolithic IMUs.

Fig. 16(a) shows a photo of a fabricated gyroscope. The die size is 6.5 mm $\times$ 7.5 mm. Fig. 16(b) shows a scanning electron microscopy (SEM) image of a closed-up view of the comb drive. The finger width and gap of the comb drive are 4.5 and 5.0 μm, respectively. The gap is about 1 μm larger than the designed value due to the DRIE CD loss. The finger length and overlap length are 50 and 20 μm, respectively, leaving a maximum travel range of 10 μm for the proof mass. Fig. 16(c) shows a SEM of a closed-up view of the torsional sensing comb.

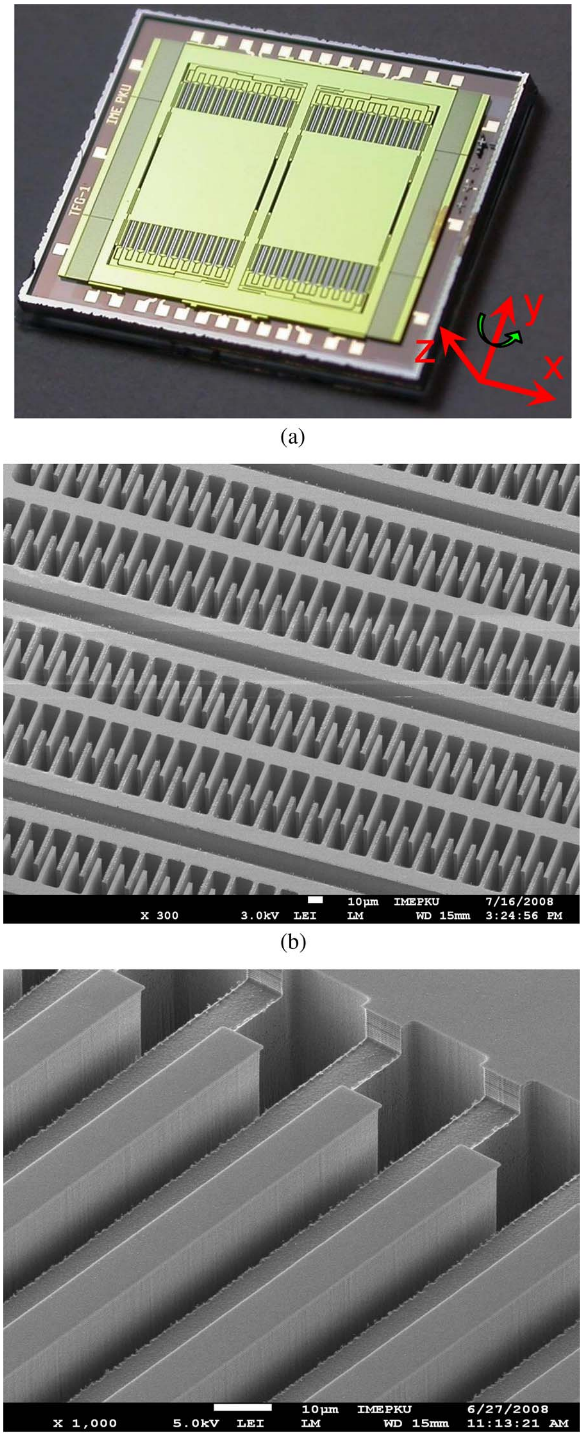

Fig. 16. (a) Photograph of the whole device. SEM images of (b) the decoupled comb drive and (c) the torsional sensing comb.

The finger width and gap are 12 and 4.5 μm, respectively. The finger height difference is 8 μm, which is about 2 μm less than the designed value.

IV. Test Results

The TFG was tested at atmospheric pressure. The frequency responses of the two working modes are shown in Fig. 17, which were tested using the dynamic analyzer Agilent35670.

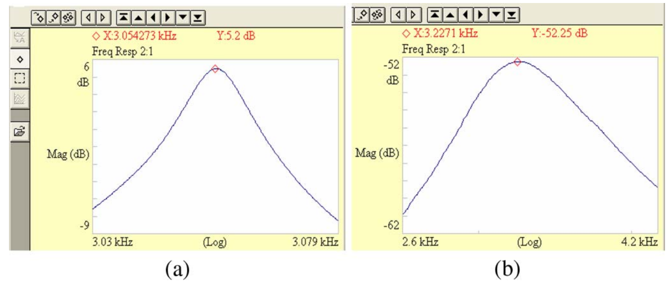

Fig. 17. Mode test. (a) Driving mode with resonant frequency $= 3.05$ kHz and $Q = 340$ and (b) sensing mode with resonant frequency $= 3.23$ kHz and $Q = 4.5$.

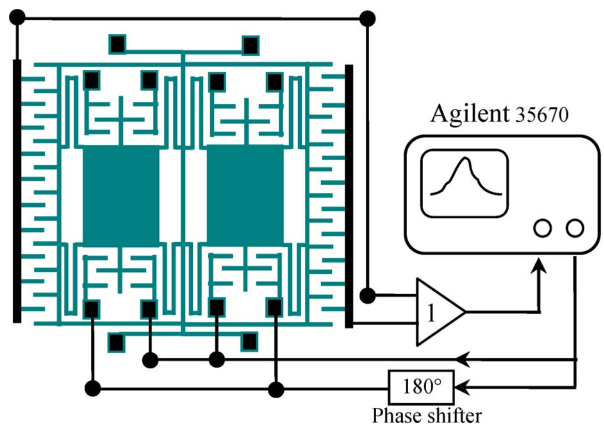

Fig. 18. Schematic of the coupling test setup of the TFG.

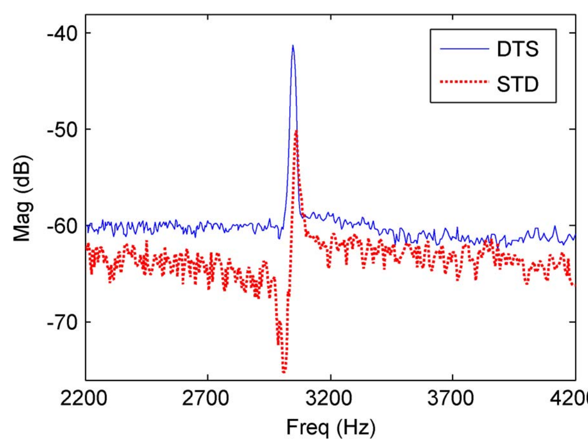

Fig. 19. Coupling test result.

The Q factor of the driving mode is 340, which is much larger than that of the sensing mode, which is only 4.5. This is because the squeezed-film damping between the proof mass and the substrate is still significant due to the large overlap area even though the gap is as large as 30 μm. Thus, improved performance can be expected when the TFG works in a vacuum environment. Perforated proof masses can also be used to lower the damping.

Fig. 18 shows the implementation of the coupling test setup. The test result of the coupling between the two working modes is shown in Fig. 19. The coupling from the driving mode to the sensing mode is -41 dB, while the coupling from the sensing mode to the driving mode is -50 dB, which indicates that the

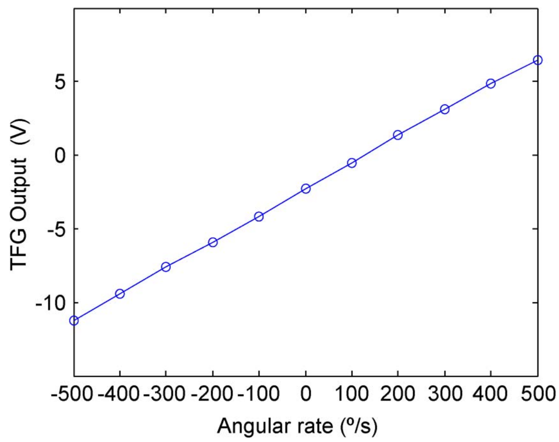

Fig. 20. Output of the TFG versus angular rate input.

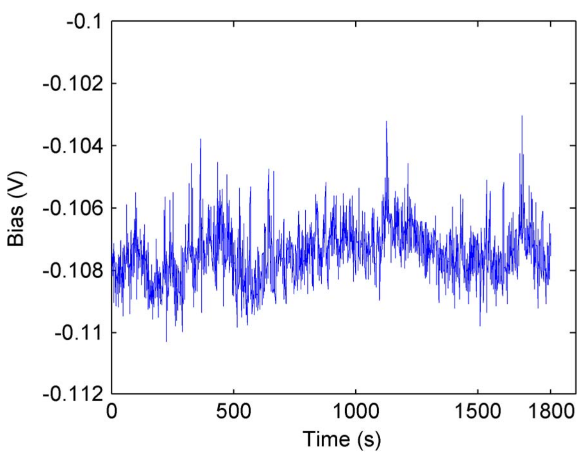

Fig. 21. Bias drift of the TFG in half an hour.

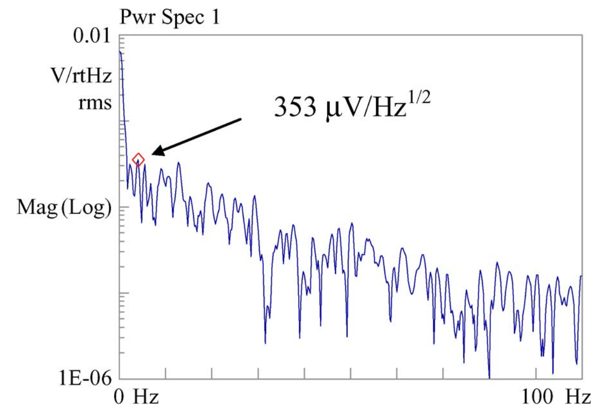

Fig. 22. Noise spectrum analysis of the TFG.

TABLE IV
PERFORMANCE OF THE LATERAL-AXIS GYROSCOPES DEVELOPED AT PKU

Year	2005 [22]	2006 [27]/ 2009 [28]	2008 [29]	2009 Vibrate wheel [31]	2009 TFG [33]	This work
Measurement range ±(°/s)	240	400	300	450	400	500
Sensitivity (mV/°/s)	0.8	6.7	3	3.1	2.9	17.8
Nonlinearity (%)	N/A	0.51	1.1	0.77	0.9	0.6
Noise (°/s/Hz$^{1/2}$)	0.1	N/A	0.1	0.45	0.035	0.02
Bias stability (°/s)	N/A	N/A	N/A	N/A	N/A	0.05
Sensitive to acceleration in principle	Y	Y	Y	N	N	N

efficiency of the decoupled comb drive is as good as that of the mechanical isolation method.

As there are several cross-coupling sources such as electrostatic, electromechanical, and mechanical couplings [18], residual cross-coupling may exist when only one decoupling method is adopted [19], which can be seen in Fig. 19. Because the mechanical isolation and decoupled comb drive can suppress most of the cross-coupling, the residual cross-coupling can be nulled by other decoupling methods such as electrostatic-force compensation [5], [9].

The scale factor, bias drift, and noise spectrum of the TFG were also tested. The schematics of the control and readout electronics of the TFG are intensively introduced in [41].

The relationship between the outputs of the TFG under different input angular rates is shown in Fig. 20. With a full range of 1000 $^\circ/\mathrm{s}$, the TFG has a sensitivity of 17.8 mV$/^\circ/\mathrm{s}$ and the nonlinearity is 0.6%. The measurement range is $\pm 500\ ^\circ/\mathrm{s}$, which is limited by the maximum angular rate of the rotating rate table. The basic sensitivity of the TFG is 31.7 aF$/^\circ/\mathrm{s}$ and the electrical gain of the capacitance/voltage converter is 3.55 μV/aF.

The output of the TFG under zero input has been recorded for approximately half an hour, as shown in Fig. 21. The standard deviation of the output under zero input is defined as the bias stability of the TFG in this paper. For 30 min, the TFG has a bias stability of 0.05 $^\circ/\mathrm{s}$ (1σ), resulting into the 86-dB dynamic range of this TFG. Considering the limit of the turntable, even higher dynamic range can be anticipated. Long-term stability and the error sources of the TFG are still needed to be investigated in the future.

Fig. 22 shows the output noise spectrum analysis after a 25-Hz cutoff low-pass filtering using the Agilent35670 analyzer. The equivalent noise angular rate is calculated to be 0.02 $^\circ/\mathrm{s/Hz}^{1/2}$.

The performance of this TFG and the performances of other lateral-axis gyroscopes developed at PKU are listed in Table IV. Overall, this TFG has the highest resolution and a good bias stability. However, the resolution of the TFG still has a large gap when compared with high-vacuum-packaged MEMS gyroscopes [5], and the bias stability is not as good as those of capacitive MEMS gyroscopes from industry [6]–[8].

V. CONCLUSION

A doubly decoupled lateral-axis micromachined TFG with decoupled comb drives and torsional sensing comb capacitors has been successfully demonstrated. Because torsional sensing area-changing comb capacitors are used and the driving mode of the gyroscope is dominated by slide-film air damping, the TFG can work even at atmospheric pressure. Due to the centroidal topology of the sensing combs, the TFG can not only differentially detect the rotational displacement but also significantly reduce the nagative effects caused by fabrication imperfections and can balance the electrostatic force along the z-axis. The TFG is fabricated with a five-mask SOG process and tested at atmospheric environment. The measured coupling from driving mode to sensing mode is -41 dB while the coupling from sensing mode to driving mode is -50 dB. The result indicates that the proposed novel comb drive can efficiently decouple the mechanical crosstalk from sensing mode to driving mode, the decoupling capability of which is proved to be as good as the mechanical insulation method used for the decoupling of driving to sensing mode. The successful combination of the two decoupling methods can simplify the structure of the sensor and also increase the effective proof mass within the same chip area, since the movable driving combs are also part of the proof mass, which is particularly important for the development of low-cost gyroscopes working at atmospheric pressure. The sensitivity is 17.8 mV/$^\circ$/s, and the nonlinearity is 0.6% with a full scale of 1000 $^\circ$/s. The bias stability in 30 min is $0.05\ ^\circ/\mathrm{s}\ (1\sigma)$, and the noise floor is $0.02\ ^\circ$/s/Hz$^{1/2}$.

However, there are some limitations to the TFG; for example, the fabrication process is more suitable for a bulk micromachining process than for a surface process as comb fingers need to be thinned on both top and bottom sides.

Although the area-changing comb capacitors can lower the air damping between the movable and fixed sensing electrodes, the quality factor of the sensing mode of the TFG is still as low as 4.5 when working at atmospheric pressure. This is because the proof masses have a very large area $(2.1 \times 2.4\ \mathrm{mm}^2)$ and the squeezed-film air damping is still significant even a large gap of 30 μm is used. To further improve the performance of the gyroscope, the gap should be increased or perforated proof masses and/or vacuum packaging could be used.

REFERENCES

[1] Z. Y. Guo, L. T. Lin, Q. C. Zhao, J. Cui, X. Z. Chi, Z. C. Yang, and G. Z. Yan, "An electrically decoupled lateral-axis tuning fork gyroscope operating at atmospheric pressure," in *Proc. MEMS*, Sorrento, Italy, Jan. 2009, pp. 104–107.

[2] N. Yazdi, F. Ayazi, and K. Najafi, "Micromachined inertial sensors," *Proc. IEEE*, vol. 86, no. 8, pp. 1640–1659, Aug. 1998.

[3] W. C. Tang, T. H. Nguyen, and R. T. Howe, "Laterally driven polysilicon resonant microstructures," *Sens. Actuators*, vol. 20, no. 1/2, pp. 25–32, Nov. 1989.

[4] J. Bernstein, S. Cho, A. T. King, A. Kourepenis, P. Maciel, and M. Weinberg, "A micromachined comb-drive tuning fork rate gyroscope," in *Proc. MEMS Conf.*, Fort Lauderdale, FL, Feb. 13–17, 1993, pp. 143–148.

[5] A. Sharma, M. F. Zaman, M. Zucher, and F. Ayazi, "A 0.1°/hr bias drift electronically matched tuning fork microgyroscope," in *Proc. MEMS Conf.*, Tucson, AZ, Jan. 13–17, 2008, pp. 6–9.

[6] R. Neul, U. Gómez, K. Kehr, W. Bauer, J. Classen, C. Döring, E. Esch, S. Götz, J. Hauer, B. Kuhlmann, C. Lang, M. Veith, and R. Willig, "Micromachined gyros for automotive applications," in *Proc. IEEE SENSORS Conf.*, 2005, pp. 527–530.

[7] J. Geen and D. Krakauer, New iMEMS Angular-Rate-Sensing Gyroscope, [Online]. Available: http://www.analog.com/library/analogdialogue/archives/37-03/gyro.html

[8] J. Geen and D. Krakauer, Integrated Dual-Axis Gyro IDG-300, [Online]. Available: http//www.invensense.com

[9] M. S. Weinberg and A. Kourepenis, "Error sources in in-plane silicon tuning-fork MEMS gyroscopes," *J. Microelectromech. Syst.*, vol. 15, no. 3, pp. 479–491, Jun. 2006.

[10] A. Kourepenis, J. Borenstein, J. Connelly, R. Elliott, P. Ward, and M. Weinberg, "Performance of MEMS inertial sensors," in *Proc. IEEE Position Location Navigation Symp.*, Palm Springs, CA, 1998, pp. 1–8.

[11] W. Geiger, B. Folkmer, U. Sobe, H. Sandmaier, and W. Lang, "New designs of micromachined vibrating rate gyroscopes with decoupled oscillation modes," *Sens. Actuators A, Phys.*, vol. 66, no. 1–3, pp. 118–124, Apr. 1998.

[12] W. Geiger, J. Merz, T. Fischer, B. Folkmer, H. Sandmaier, and W. Lang, "The silicon angular rate sensor system DAVED," *Sens. Actuators A, Phys.*, vol. 84, no. 3, pp. 280–284, Sep. 2000.

[13] W. Geiger, W. U. Butt, A. Gainer, J. Frech, M. Braxmaier, T. Link, A. Kohne, P. Nommensen, H. Sandmaier, and W. Lang, "Decoupled microgyros and the design principle DAVED," *Sens. Actuators A, Phys.*, vol. 95, no. 2/3, pp. 239–249, Jan. 2002.

[14] H. Kawai, K.-I. Atsuchi, M. Tamura, and K. Ohwada, "High-resolution microgyroscope using vibratory motion adjustment technology," *Sens. Actuators A, Phys.*, vol. 90, no. 1/2, pp. 153–159, May 2001.

[15] S. Park and R. Horowitz, "Adaptive control for the conventional mode of operation of MEMS gyroscopes," *J. Microelectromech. Syst.*, vol. 12, no. 1, pp. 101–108, Feb. 2003.

[16] C. C. Painter and A. M. Shkel, "Active structural error suppression in MEMS vibratory rate integrating gyroscopes," *IEEE Sensors J.*, vol. 3, no. 5, pp. 595–606, Oct. 2003.

[17] A. S. Phani, A. A. Seshia, M. Palaniapan, R. T. Howe, and J. A. Yasaitis, "Modal coupling in micromechanical vibratory rate gyroscopes," *IEEE Sensors J.*, vol. 6, no. 5, pp. 1144–1152, Oct. 2006.

[18] N. Wakatsuki, M. Ono, S. Yamada, K. Kikuchi, and M. Yamauchi, "Suppression of null signals in LiTaO3 crystal fork vibratory gyroscope," in *Proc. IEEE Ultrasonics Symp.*, 1995, pp. 424–427.

[19] M. Braxmaier, A. Gaiber, A. Schumacher, I. Simon, J. Frech, H. Sandmaier, and W. Lang, "Cross-coupling of the oscillation modes of vibratory gyroscopes," in *Proc. Int. Conf. Solid State Sens., Actuators, Microsyst.*, Boston, MA, Jun. 2003, pp. 167–170.

[20] Z. C. Yang, C. S. Wang, G. Z. Yan, Y. Hao, and G. Wu, "A bulk micromachined lateral axis gyroscope with vertical sensing comb capacitors," in *Proc. Transducers Conf.*, Seoul, Korea, Jun. 5–9, 2005, pp. 121–124.

[21] A. Selvakumar and K. Najafi, "A high-sensitivity z axis capacitive silicon microaccelerometer with a torsional suspension," *J. Microelectromech. Syst.*, vol. 7, no. 2, pp. 192–200, Jun. 1998.

[22] Z. C. Yang, G. Z. Yan, Y. L. Hao, and G. Y. Wu, "Design and fabrication of a torsional z-axis capacitive accelerometer with novel comb capacitor," in *Proc. 7th Int. Conf. Solid-State Integr. Circuits Technol.*, Oct. 18–21, 2004, pp. 1792–1795.

[23] T. Tsuchiya and H. Funabashi, "A Z-axis differential capacitive SO1 accelerometer with vertical comb electrodes," in *Proc. IEEE MEMS*, Maastricht, The Netherlands, Jan. 25–29, 2004, pp. 524–527.

[24] H. K. Xie and G. Fedder, "A CMOS z-axis capacitive accelerometer with comb-finger sensing," in *Proc. IEEE MEMS*, Miyazaki, Japan, Jan. 23–21, 2000, pp. 496–501.

[25] C. C. Chu, J. U. Tsai, J. Hsieh, and W. L. Fang, "A novel electrostatic vertical comb actuator fabricated on (111) silicon wafer," in *Proc. 16th MEMS*, Kyoto, Japan, Jan. 19–23, 2003, pp. 56–59.

[26] K. Jongpal, P. Sangjun, K. Donghun, K. Hyouingho, and D. D. Cho, "An x-axis single-crystalline silicon microgyroscope fabricated by the extended SBM process," *J. Microelectromech. Syst.*, vol. 14, no. 3, pp. 444–455, Jun. 2005.

[27] X. Liu, Z. Yang, G. Yan, J. Fan, H. Ding, and Y. Liu, "Design and fabrication of a lateral axis gyroscope with asymmetric comb-fingers as sensing capacitors," in *Proc. NEMS*, Zhuhai, China, Jan. 18–21, 2006, pp. 762–765.

[28] J. Cui, X. S. Liu, Q. C. Zhao, L. T. Lin, X. Z. Chi, Z. C. Yang, and G. Yan, "An investigation of decoupling performance for a novel lateral axis gyroscope with varying environmental parameters," in *Proc. Transducers Conf.*, Denver, CO, Jun. 21–29, 2009, pp. 292–295.

[29] X. S. Liu, Z. C. Yang, X. Z. Chi, J. Cui, H. T. Ding, Z. Y. Guo, B. Lv, and G. Z. Yan, "A X-axis micromachined gyroscope with doubly decoupled oscillation modes," in *Proc. MEMS Conf.*, Tucson, AZ, Jan. 13–17, 2008, pp. 860–863.

[30] X. S. Liu, Z. C. Yang, X. Z. Chi, J. Cui, H. T. Ding, Z. Y. Guo, B. Lv, L. T. Lin, Q. C. Zhao, and G. Z. Yan, "A doubly decoupled lateral axis micromachined gyroscope," *Sens. Actuators A, Phys.*, vol. 154, no. 2, pp. 218–233, Sep. 2009.

[31] Q. C. Zhao, X. S. Liu, L. T. Lin, Z. Y. Guo, J. Cui, X. Z. Chi, Z. C. Yang, and G. Z. Yan, "A doubly decoupled micromachined vibrating wheel

gyroscope," in *Proc. Transducers Conf.*, Denver, CO, Jun. 21–29, 2009, pp. 296–299.

[32] Z. Y. Guo, Z. C Yang, L. T. Lin, Q. C. Zhao, J. Cui, X. Z. Chi, and G. Z. Yan, "A lateral-axis micromachined tuning fork gyroscope with novel driving and sensing combs," in *Proc. Transducers Conf.*, Denver, CO, Jun. 21–29, 2009, pp. 288–291.

[33] Z. Y. Guo, Z. C Yang, L. T. Lin, Q. C. Zhao, H. T. Ding, X. S. Liu, J. Cui, H. Xie, and G. Z. Yan, "A lateral-axis micromachined tuning fork gyroscope with torsional Z-sensing and electrostatic force-balanced driving," *J. Micromech. Microeng.*, vol. 20, no. 2, p. 025 007, Feb. 2010.

[34] Z. H. Li, Z. C. Yang, Z. X. Xiao, Y. L. Hao, T. Li, G. Y. Wu, and Y. Y. Wang, "A bulk micromachined vibratory lateral gyroscope fabricated with wafer bonding and deep trench etching," *Sens. Actuators A, Phys.*, vol. 83, no. 1–3, pp. 24–29, May 2000.

[35] F. Braghin, F. Resta, E. Leo, and G. Spinola, "Nonlinear dynamics of vibrating MEMS," *Sens. Actuators A, Phys.*, vol. 134, no. 1, pp. 98–108, Feb. 2007.

[36] J.-L. A. Yeh, C.-Y. Hui, and N. C. Tien, "Electrostatic model for an asymmetric combdrive," *J. Microelectromech. Syst.*, vol. 9, no. 1, pp. 126–135, Mar. 2000.

[37] Z. Y. Guo, Z. C. Yang, L. T. Lin, Q. C. Zhao, J. Cui, X. Z. Chi, and G. Z. Yan, "Decoupled comb capacitors for microelectromechanical tuning-fork gyroscopes," *IEEE Electron Device Lett.*, vol. 31, no. 1, pp. 26–28, Jan. 2010.

[38] B. Lv, X. S. Liu, Z. C. Yang, and G. Z. Yan, "Simulation of a novel lateral axis micromachined gyroscope in the presence of fabrication imperfections," *Microsyst. Technol.*, vol. 14, no. 6, pp. 711–718, Jun. 2008.

[39] X. S. Liu, C. W. Wang, Y. Zhu, and G. Z. Yan, "Vertical profiles and CD loss control in deep RIE technology," in *Proc. 7th Int. Conf. Solid-State Integr. Circuits Technol.*, Oct. 18–21, 2004, vol. 3, pp. 1848–1851.

[40] I. W. Rangelow, "Critical tasks in high aspect ratio silicon dry etching for microelectromechanical systems," *J. Vac. Sci. Technol. A, Vac. Surf. Films*, vol. 21, no. 4, pp. 1550–1562, Jul./Aug. 2003.

[41] J. Cui, X. Z. Chi, H. T. Ding, L. T. Lin, Z. C. Yang, and G. Z. Yan, "Transient response and stability of the AGC-PI closed-loop controlled MEMS vibratory gyroscopes," *J. Micromech. Microeng.*, vol. 19, no. 12, p. 125 015, Dec. 2009.

Zhong Yang Guo received the B.S. degree in mechanical engineering from Yanshan University, Qinhuangdao, China, in 1997, the M.S. degree in automatic control engineering from the Beijing Institute of Automatic Control Equipment, Beijing, China, in 2002, and the Ph.D. degree in microelectronics from Peking University, Beijing, in 2010.

He is currently a Postdoctor with Peking University. His research interests are in the area of microelectromechanical-system technology.

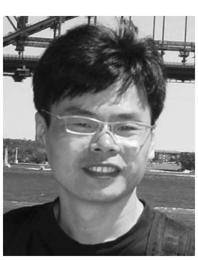

Long Tao Lin received the B.S. and M.S. degrees in mechanical engineering from the Harbin Institute of Technology, Harbin, China, in 2001 and 2003, respectively.

Then, he was with the Beijing Institute of Computer Application and Simulation Technology, Beijing, China. In 2006, he joined the Institute of Microelectronics, Peking University, Beijing, as a Technical Staff. His research interest focuses on the design of readout circuits for microelectromechanical-system sensors.

Qian Cheng Zhao received the B.S. degree in mechanical engineering from the Harbin Institute of Technology, Harbin, China, in 1998 and the M.S. and Ph.D. degrees from Peking University, Beijing, China, in 2007.

He is currently a Postdoctor with Peking University. His research interests are in the area of microelectromechanical-system technology.

Zhen Chuan Yang received the B.S. and Ph.D. degrees from the School of Electronic Engineering and Computer Science, Peking University, Beijing, China, in 1998 and 2004, respectively.

From August 2004 to June 2006, he was a Research Associate with the Department of Electronic and Computer Engineering, The Hong Kong University of Science and Technology, Clear Water Bay, Hong Kong, engaging in research works on GaN-based microelectromechanical-system (MEMS) devices. In July 2006, he joined the Institute of Microelectronics, Peking University, where he is currently an Associate Professor. His research interests include micromachined inertial sensors, monolithic integration processes, and GaN-based MEMS devices.

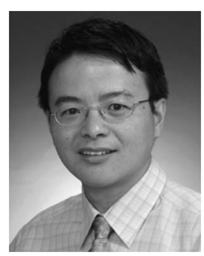

Huikai Xie (S'00–M'02–SM'07) received the B.S. and M.S. degrees in electronic engineering from the Beijing Institute of Technology, Beijing, China, the M.S. degree in electrooptics from Tufts University, Boston, MA, in 1998, and the Ph.D. degree in electrical and computer engineering from Carnegie Mellon University, Pittsburgh, PA, in 2002.

He is an Associate Professor with the Department of Electrical and Computer Engineering, University of Florida, Gainesville. From 1992 to 1996, he was a Faculty Member with the Institute of Microelectronics, Tsinghua University, Beijing, working on various silicon-based chemical and mechanical sensors. He has published over 100 technical papers. He is the holder of four U.S. patents granted and eight U.S. patents pending. His present research interests include micro-/nanofabrication, integrated microsensors, gyroscopes, wireless sensors, microelectromechanical-system (MEMS) inductors, optical MEMS, biomedical imaging, and biophotonics.

Gui Zhen Yan received the B.S. degree in microelectronics from Peking University, Beijing, China, in 1974.

She is currently a Professor with the Institute of Microelectronics, Peking University. Her research interests include design and fabrication of microelectromechanical-system (MEMS) inertial sensors, monolithic integration of bulk MEMS sensors, and ICs. She has published more than 150 technical papers and has filed about 20 patents.